# LEAN BLOWOUT (LBO) SIMULATIONS IN A RICH-BURN QUICK-QUENCH LEAN-BURN (RQL) GAS TURBINE COMBUSTOR

**C. Thomas Wey**

NASA Glenn Research Center, Cleveland, OH, USA

## ABSTRACT

*The transient processes involving lean blowout (LBO) in a RQL combustor such as the single cup combustor in the National Jet Fuels Combustion Program (NJFCP) referee rig are simulated with the reduced mechanisms based on Hybrid Chemistry for two different fuels, Cat-A2 and Cat-C1. Cat-A2 fuel is Jet-A with average or nominal properties based on a survey of the Petroleum Quality Information System database. The Cat-C1, an alternative jet fuel, is a GEVO alcohol-to-jet (ATJ) fuel composed almost entirely of two highly-branched C12 and C16 iso-paraffins. Experiments conducted in the NJFCP referee rig established a stable flame at an equivalence ratio of 0.096 (the near LBO condition) as the starting condition for LBO tests performed with all Category A and C fuels. Simulations of the approach to LBO verify that a stable flame is established at the near-LBO condition for each fuel before reducing fuel flow rate (and thus equivalence ratio) in a step-wise manner. At each new equivalence ratio, the global heat release rate and total fuel evaporation time histories are monitored to verify a new stable flame condition has been established before performing the next reduction in equivalence ratio until the flame is approaching the blowout. Main conclusions are threefold: (1) For Cat-C1 fuel the equivalence ratio for LBO is around 0.087. (2) For Cat-A2 fuel the equivalence ratio for LBO is either 0.082 or 0.078 depended on the time span of equivalence ratio of 0.085. (3) The averaged difference from LES on LBO for Cat-C1 relative to Cat-A2 is 8.75% versus 7.8% from the experimental data.*

Keywords: Lean blow out. LES, high-order SLAU2 scheme, fuel sensitivity.

## NOMENCLATURE

| | |
|---|---|
| LBO | lean blow out |
| NBO | near lean blow out |
| NJFCP | National Jet Fuels Combustion Program |
| $\phi$ | equivalence ratio |

## 1. INTRODUCTION

Recent more stringent emission standards have enticed the development of more fuel-efficient and low-emission combustion system for aircraft gas turbine applications. There is also interest in producing “alternative jet fuels” from various non-petroleum sources that consist solely of hydrocarbons and that provide essentially identical performance to that from petroleum-derived jet fuels. However, the cost is high to develop the technical data for the acceptance of the fuel standards. While these alternative jet fuels must meet current requirements for key parameters such as heat release, there are many other factors to be examined before accepting each alternative jet fuel for aviation use, including combustor operability characteristics, such as lean blowout (LBO), cold start, and high-altitude relight. In the present work, the transient processes involving lean blowout (LBO) in a RQL combustor such as the single cup combustor in the National Jet Fuels Combustion Program (NJFCP) referee rig [1] are simulated with the reduced mechanisms based on Hybrid Chemistry [2] for two different fuels3, Cat-A2 and Cat-C1. Cat-A2 fuel is Jet-A with average or nominal properties based on a survey of the Petroleum Quality Information System database. The Cat-C1, an alternative jet fuel, is a GEVO alcohol-to-jet (ATJ) fuel composed almost entirely of two highly-branched C12 and C16 iso-paraffins and will distillate 80% of its components at temperatures less than 200$^{o}$C (while A2 requires temperatures of 230$^{o}$C or above to distillate 80% of its components) [3].

NJFCP has been working to create a more streamlined procedure for approving alternative jet fuels to be used by the aviation industry. The fuel sensitivity of LBO, cold start and high-altitude ignition are the combustor operability issues of most concern.

Developing a comprehensive reacting LES strategy of applying the OPENNCC code to the realistic gas turbine combustors for LBO, flashback, and combustion dynamics is currently underway. The current effort considers LBO fuel sensitivity. Experiments conducted in the NJFCP referee rig established a stable flame at an equivalence ratio ($\phi$) of 0.096 (the near LBO condition) as the starting condition for LBO tests performed with all Category A and C fuels. Simulations of the approach the LBO verify that a stable flame is established at the near-LBO condition for each fuel before reducing fuel flow rate (and thus $\phi$) in a step-wise manner.

The open source version (OpenNCC) of National Combustion Code (NCC) currently under-development at NASA Glenn Research Center will be used for the calculations. OpenNCC adopts the data structure of arbitrary polyhedrons that permit cells of arbitrary shape to be used: cells can have an arbitrary number of faces and faces can have an arbitrary number of points. A brief summary of the code is listed here. The code solves the compressible Navier-Stokes equation while the preconditioning is optional for simulating the low Mach number flow. A second order accurate central or upwind scheme is used for spatial discretization of the Euler fluxes in LES governing equations. A third order accurate central or upwind scheme is available as well via Taylor series expansion for spatial discretization of the Euler fluxes. For a typical spray reacting simulation, the third order SLAU [4] flux splitting method for the inviscid flux requires 40 percent more computer-time compared against that of the second order SLAU2 scheme. A second order accurate central scheme is used for discretization of the Laplacian terms in the governing equations. For the temporal integration, the options include: (1) non-iterative second order predictor-corrector MacCormack scheme; (2) noniterative global-time-step multi-stage Runge-Kutta scheme; (3) dual-time sub-iterative 3-4-5-stage Runge-Kutta scheme. Four available turbulence models in the code are summarized in Table 1 from the coding point of view.

| Turbu-lence Model | Turbu-lence Stresses | Eddy Vis cosity | K-Destruction Term | Coefficients |
|---|---|---|---|---|
| TFNS | Quadratic & Cubic | $C_\mu \rho K^2/\varepsilon$ | $\rho\varepsilon$ | RCP: Prescribed |
| K – LES | Linear | $C_\nu \rho K^{0.5}\Delta$ | $C_\varepsilon \rho (K)^{1.5}/\Delta$ | $C_\nu$, $C_\varepsilon$: Prescribed or computed by LDKM scheme or an empirical formula |
| LES | Linear | $(C_s\Delta)^2\rho\|S\|$ | N/A | $C_s$, Prescribed |
| TFNS /LES | Quadratic & Cubic | Min($C_\mu \rho K^2/\varepsilon$, $(C_s\Delta)^2\rho\|S\|$) | Max($\rho\varepsilon$, $C_\varepsilon \rho (K)^{1.5}/\Delta$) | RCP: Prescribed $C_\varepsilon$, $C_s$: Prescribed |

**Table 1** Turbulence Models in the code. (K-LES model is used for the current simulations.)

The liquid spray solver is based on a Lagrangian scheme and various well-established models for droplet drag; the Frossling [5] and Faeth [6] vaporization models coupled with the constant droplet internal heating and it employs models for gas-film valid over a wide range of low to intermediate droplet Reynolds numbers.

Previously all the necessary mesh, inputs and some preliminary simulations have been reported in Reference 7, however the results in that report were incomplete and thus inconclusive. This study attempts to complete the LBO efforts.

## 2. RESULTS AND DISCUSSION

A patched mesh of 12,640,138 hexahedrons (provided by UTRC through Ga Tech) was acquired to study approach to lean blowout for this combustor. The mesh is patched together by nine blocks. The mesh resolutions are not too compatible between blocks. The interface among the blocks is mainly achieved by linear interpolation of the primitive variables.

The injection system consists of two outer axial swirlers and an inner radial swirler with a pressure-swirl atomizer nested in the center (See Figure 1). The atomizer and the radial swirler are located upstream of the exit plane of the axial swirlers. Dilution holes are located at two axial positions along upper and lower walls of combustor with three holes at the first row (45 mm downstream of the injector exit plane), and four holes at the second row further downstream. The LBO tests start at a stable flame condition near LBO (207000 Pa combustion chamber pressure and overall equivalence ratio of 0.096) and the lower the fuel flow rate in controlled and repeatable manner until LBO occurs (determined by the rapid drop of the signal from a photodiode directed at the combustor primary zone). The average time required to ramp the fuel down to LBO during actually testing was typically 200-300 sec.

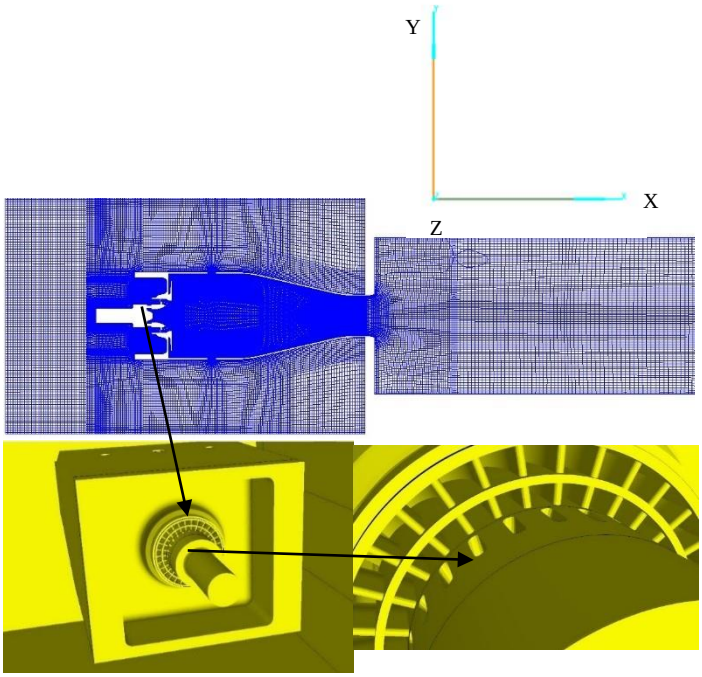


**FIGURE 1** A middle plane cut of the patched grid. Number of elements is 12,640,138 hexahedrons.

Injection system consists of two outer axial swirlers and an inner radial swirler. The resolutions of the meshes between the patched grids are barely compatible. A represented plot of the grid is shown in Figure 1. At the inlet, the air mass flow rate of is 0.3914 kg/s, the static temperature is 394 K. The back pressure at the exit of the extended outlet block is set to 207,000 Pa. All walls are no-slip and adiabatic. The mass flow split between the three swirlers and the two rows of the dilution holes is computed at the locations shown in Figure 2. However, the experimental flow split data are collected for the non-reacting conditions only.

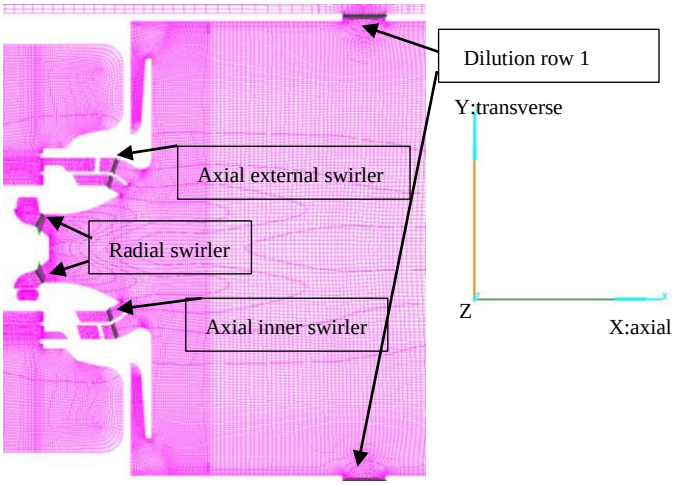


**FIGURE 2** Locations of the mass flow split computed by the code.

The uniform effusion cooling conditions at the combustor dome are 3.216 kg/s per $m^2$ (0.0250 kg/s) and 394 K on one side of the walls and -5.3802 kg/s per $m^2$ (-0.0250 kg/s) on the other side of walls since the size of wall areas are different. Similarly, the uniform effusion cooling conditions at: (1) the forward liner are 3.1608 kg/s per $m^2$ (0.04188 kg/s) and 394k versus -1.6618 kg/s per $m^2$ (-0.04188 kg/s) and 394 K, (2) the middle liner are 2.92 kg/s per $m^2$ (0.04266 kg/s) and 394 K versus -2.3797 kg/s per $m^2$ (-0.04266 kg/s)and 394 K, (3) the aft liner are 2.2679 kg/s per $m^2$ (0.06575 kg/s) and 394 K, versus -1.8867 kg/s per $m^2$ (-0.06575 kg/s) and 394 K, (4) the side slot liner are 46.53 kg/s per $m^2$ (0.06575 kg/s) and 394 K versus -46.53 kg/s per $m^2$ (- 0.06575 kg/s) and 394 K. For simplicity, in the current work, the mass flow from the side slot liner has been folded into the aft liner. The total mass flow rate for the entire combustor is 0.3914 kg/s after in and out cancellations for the effusion-cooling boundary conditions. The boundary conditions used are the same as those of the benchmark operating conditions for the AFRL referee rig.

### 2.1 Cat-C1 fuel

The starting equivalence ratio selected for Cat-C1 fuel is 0.096. It is a rather steady operating condition reported from the experimental data. The averaged formula of the Cat-C1 (Designation of POSF11498) is represented by $C_{12.6}H_{27.2.}$
A reduced hybrid chemistry (HyChem) model [8] is used for the mechanism of the real Cat-C1 fuel. The non-stiff version of the reduced mechanism consists of 26 species and 182 reactions for the purpose of lowering the cost of the finite chemistry simulations. The liquid properties are prescribed from T. Edward experimental database [3,9] that includes the density, heat capacity, viscosity and latent heat of vaporization, shown in Table 2. The gas properties are prescribed from H. Wang's HyChem model [8].

| Liquid Physical Properties | Units | Cat-A2 | Cat-C1 |
|---|---|---|---|
| Density | $Kg/M^3$ | -0.74617*T+1018.26 | -0.72*T+967.01 |
| Heat Capacity | J/Kg/K | 4.28*T + 723.0 | 4.10*T+753.0 |
| Viscosity | Pa-S | 0.08949*exp(0.01394*T) | 1.89212* exp(-0.02393*T) |
| Vapor Pressure | Pa | 10.**(28.95-3000.4/T6.5*log10(T)-0.0004*T) | 10.**(28.9-3000.4/T-6.5*log10(T)-0.0004*T) |
| Latent Heat | J/Kg | $380000*[(T_c-T)/(T_c-298]_{0.375}$ | $360000*[(T_c-T)/(T_c-298]_{0.375}$ |
| Critical Temperature | K | 760.4 | 740.2 |

**Table 2** Liquid physical properties fitted in terms of temperature.

The spray boundary conditions applied are briefly described here. The liquid boundary conditions are created such that at 2 mm downstream of the physical fuel injector, there are six rings of distinguished spray droplets formed. Each ring has its (1) cumulative distribution function for initial sizes of spray drops computed by inverse transform sampling (i.e. SMD is not used directly.), (2) inner and outer injection angles of the ring, (3) represented SMD computed from CDF as a reference but not used, (4) fuel particle speed, (5) fuel mass flow rate.

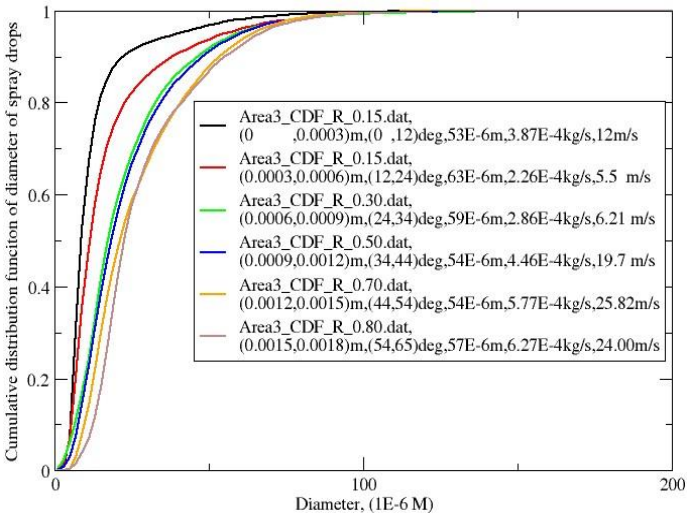


**FIGURE 3** CDF from Purdue PDPA spray measurements and spray boundary conditions.

A middle plane cut of time-averaged axial velocity and averaged axial recirculation velocity are shown in Figure 4(a) and (b)

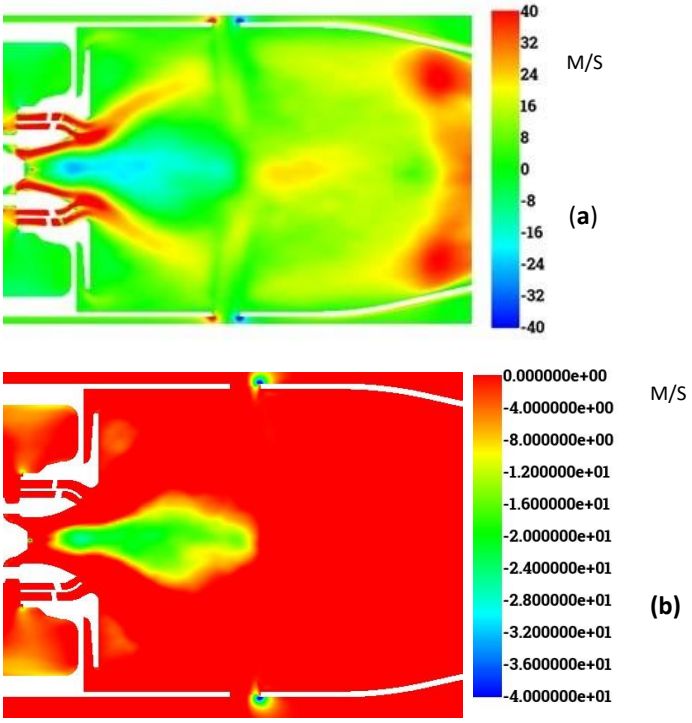


In Figure 4(c), the time-averaged speed on a middle plane cut is shown. The bending of the dilution jets is noticeable.

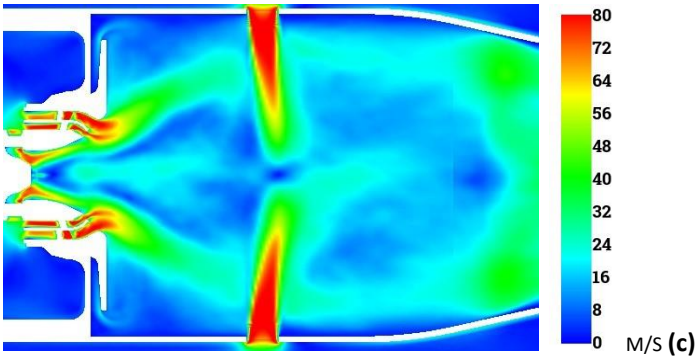


**FIGURE 4** A middle plane cut of (a) time average axial velocity and (b) time average axial central recirculation velocity (c) time average velocity magnitude of Cat-C1 fuel at $\phi = 0.096$.

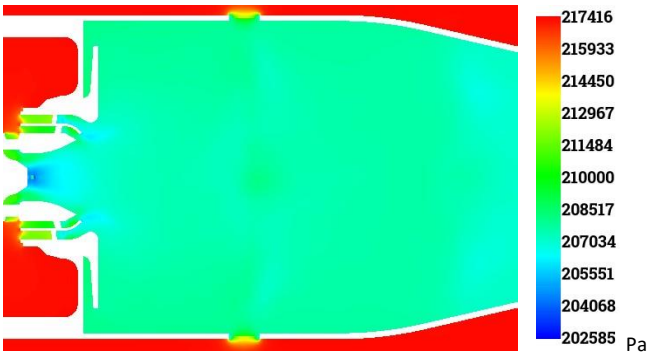


**FIGURE 5** A middle plane cut of average pressure.

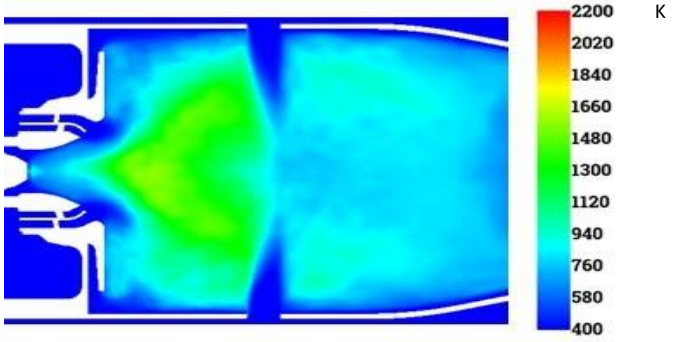


**FIGURE 6** A middle plane cut of average temperature.

From Figures 4 to 6, the contours of time-averaged pressure and temperature in a central plane cut normal to the z axis are shown respectively. The higher speed accelerated in the exit area of the aft-combustor could be contributed due to the chemical mechanism used. The pressure distribution in the aft-combustor compartment is quite uniform. The temperature distribution in the combustor is somewhat unsymmetrical and one higher temperature zone exists in lower portion of the combustor. The values of the temperature drop very quickly from the first row of the dilution hole to the second row of the dilution hole.

The time-averaged C1 mass fraction is shown in Figure 7. It shows that the injected liquid fuel is mainly vaporized in the swirler cup due to well organized recirculation zone shown in the (b) panel of Figure 3.

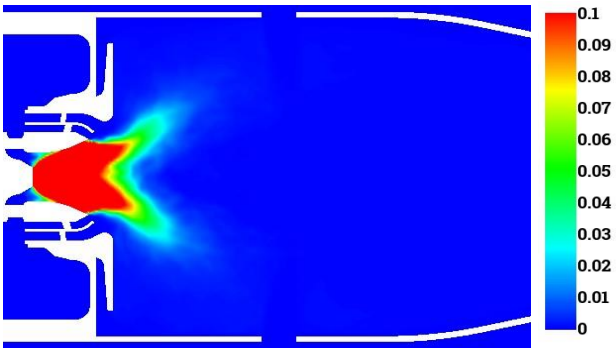


**FIGURE 7** Time-averaged Cat-C1 mass fraction in a central z normal plane cut.

The time-averaged OH mass fraction is shown in Figure 8.

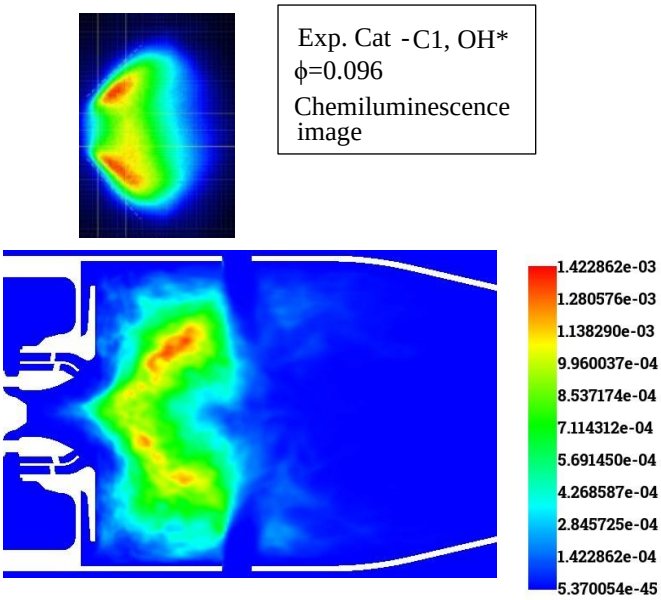


**FIGURE 8** Time-averaged LES OH mass fraction. (OH* is not available from LES predictions.)

Temporal efficiencies of C1 fuel evaporations, heating rate and T4 for $\phi$=0.096 are shown in Figure 9 respectively. It is shown that the operating condition at $\phi$=0.096 is stable.

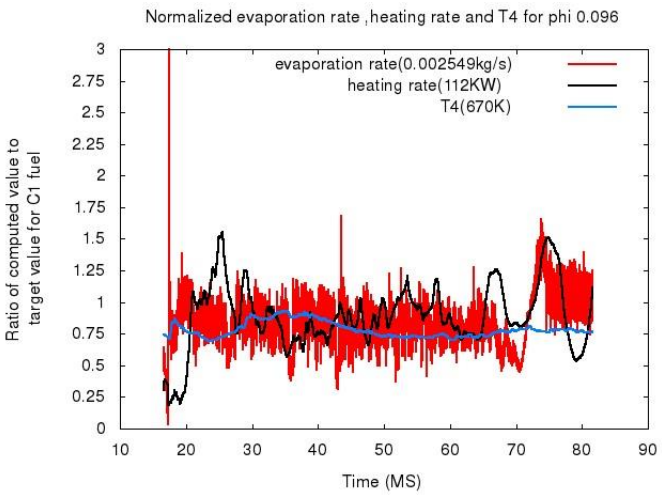


**FIGURE 9** Temporal efficiency of Cat-C1 fuel evaporations, heating rate and $T_4$ at $\phi$=0.096.

Simulations with reduced equivalence ratio, $\phi$=0.093, starts around 52 MS from the results of $\phi$=0.096. Then the equivalence ratio steps down to 0.090 after 13 MS stable simulations $\phi$=0.093. After another 13 MS stable simulations of $\phi$=0.090, the equivalence ratio steps down to 0.087. After 8 MS with $\phi$=0.087, the unsteady heating rate reduces to around 0 KW which is about 100% lost compared to the targeted value, 101.4 KW. The approach to LBO is achieved when the equivalence ratio is 0.087 for Cat-C1 fuel.

The LBO equivalence ratio from the experimental data is between 0.0861 and 0.087661. In Figure 10, the normalized unsteady heat release rates at different step-wise equivalence ratio are shown. (Note: the targeted heating rate is different from each other.) The instantaneous temperature contours with $\phi$=0.087 at 86 MS in shown in Figure 11.

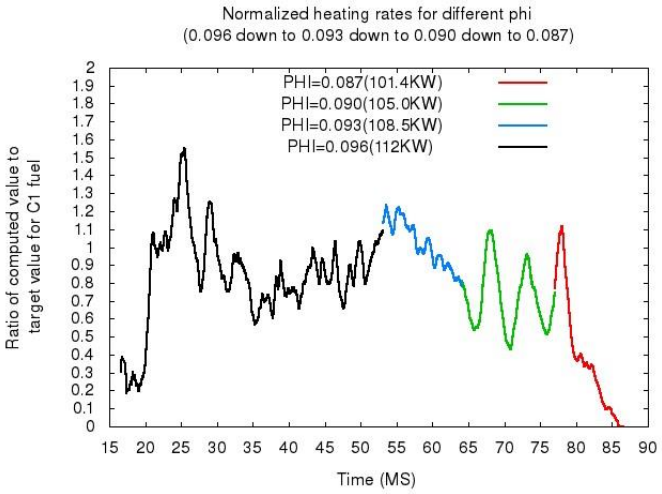


**FIGURE 10** Normalized temporal heating rates of Cat-C1 fuel with step-down $\phi$.

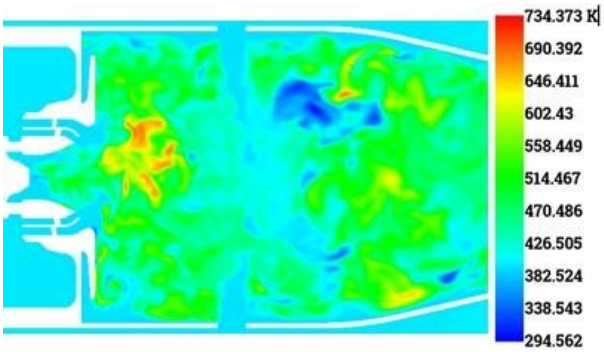


**FIGURE 11** Instantaneous center-plane temperature contours around 86 MS at $\phi$=0.087.

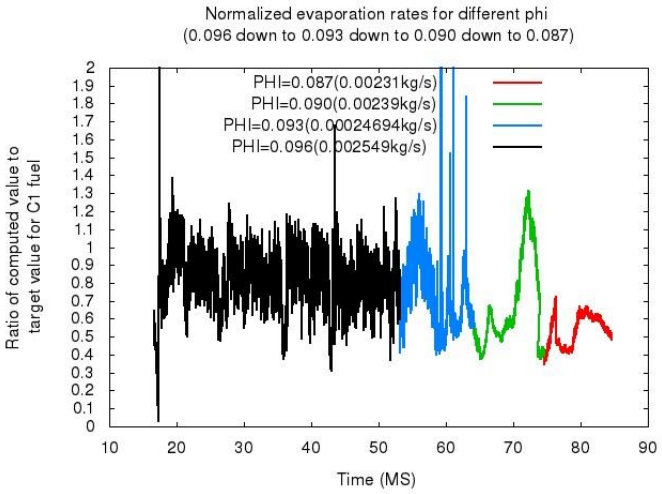


**FIGURE 12** Normalized temporal fuel evaporation rates of CatC1 fuel with step-down $\phi$.

In Figure 12, the normalized unsteady evaporation rates at different step-wise equivalence ratio are shown. (Note: the targeted evaporation rate is different from each other.)

### 2.2 Cat-A2 fuel

The averaged formula of the Cat-A2 (Designation of POSF11498) is represented by $C_{11.4}H_{21.7}$. A reduced hybrid chemistry (HyChem) model [8] is used for the mechanism of the real Cat-A2 fuel. The non-stiff version of the reduced mechanism consists of 31 species and 202 reactions for the purpose of lowering the cost of the finite chemistry simulations. The liquid properties are prescribed from T. Edward experimental database [3] that includes the density, heat capacity, viscosity and latent heat of vaporization, shown in Table 2. The gas properties are prescribed from H. Wang's HyChem model [8]. The spray boundary conditions applied are the same as before. The starting equivalence ratio selected for Cat-A2 fuel is 0.096 for the stable operating condition.

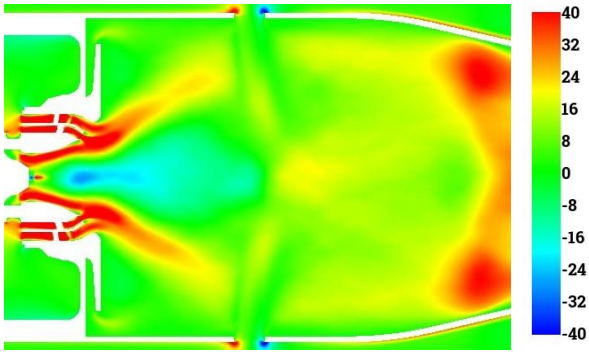


**(a)** M/S

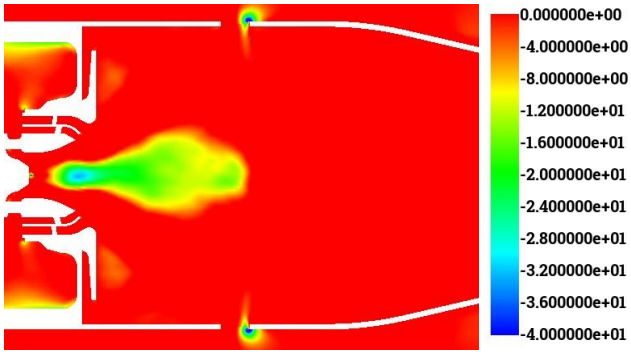


**(b)** M/S

**FIGURE 13** A middle plane cut of (a) time average axial velocity and (b) time average axial central recirculation velocity of Cat-A2 fuel at $\phi$=0.096.

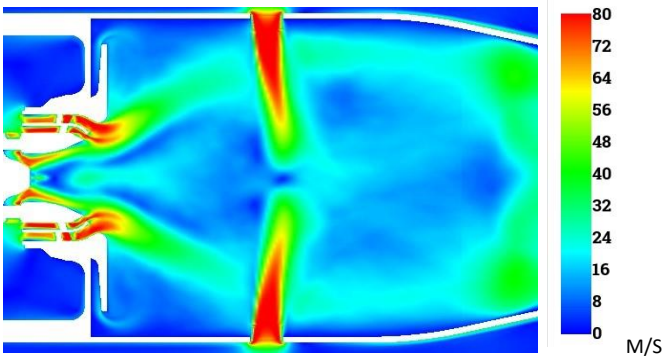


**FIGURE 14** Velocity magnitude in a central z-normal plane cut.

A middle plane cut of time-averaged axial velocity and averaged axial recirculation velocity are shown in (a) and (b) panels of Figure 13. In Figure 14, the time-averaged speed on a middle plane cut is shown. The bending of the dilution jets is noticeable. The higher speed accelerated in the exit area of the aft-combustor could be contributed due to the chemical mechanism used.

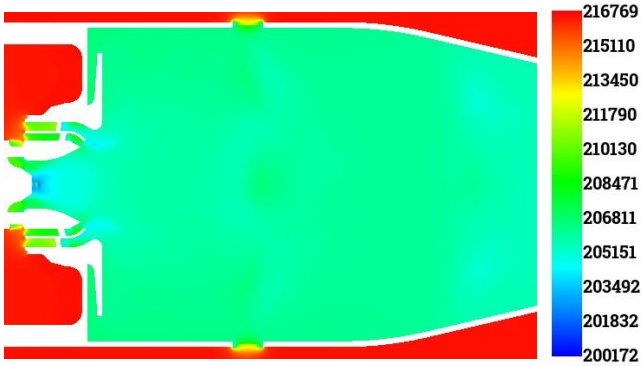


**FIGURE 15** A middle plane cut of average pressure (Pa).

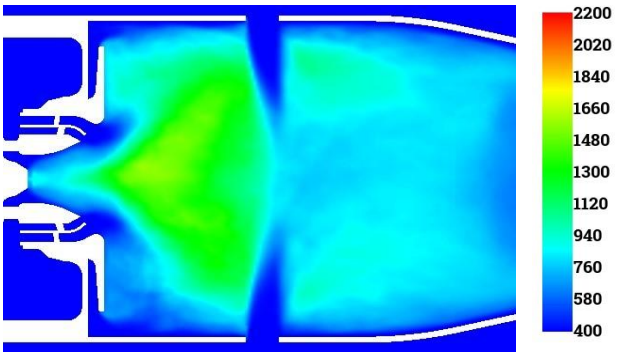


**FIGURE 16** A middle plane cut of average temperature (K).

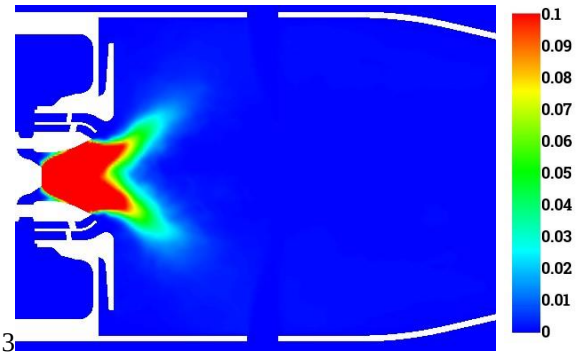


3

**FIGURE 17** Time-averaged Cat-A2 mass fraction in a central z-normal plane cut.

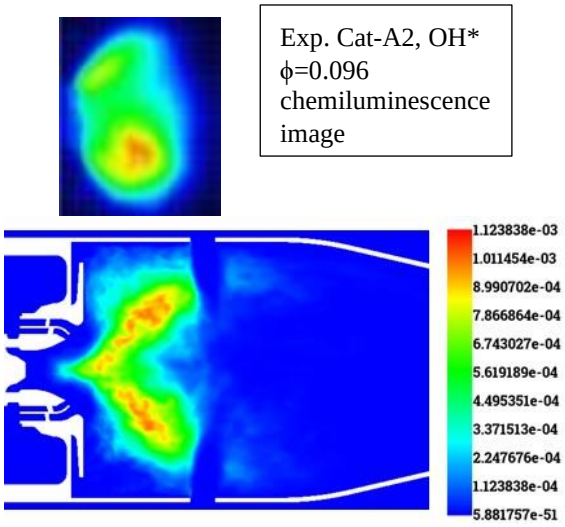


**FIGURE 18** Time-averaged LES OH mass fraction. (OH* is not available from LES predictions.)

From Figures 15 to 16, the contours of time-averaged pressure and temperature in a central plane cut normal to the z axis are shown respectively. The pressure distribution in the aft-combustor compartment is quite uniform. The temperature distribution in the combustor is somewhat unsymmetrical and one higher temperature zone exists in lower portion of the combustor. The values of the temperature drop very quickly from the first row of the dilution hole to the second row of the dilution hole. The time-averaged A2 mass fraction is shown in Figure 17. It shows that the injected liquid fuel is mainly vaporized in the swirler cup due to well organized recirculation zone shown in the (b) panel of Figure 13. The time-averaged OH mass fraction and experimentally measured OH* PLIF are shown in Figure 18. In Figure 19, the temporal efficiencies of normalized fuel evaporations, heating rate and $T_4$ for $\phi$=0.096 are shown respectively. It is clearly shown that the operating condition at $\phi$=0.096 is stable.

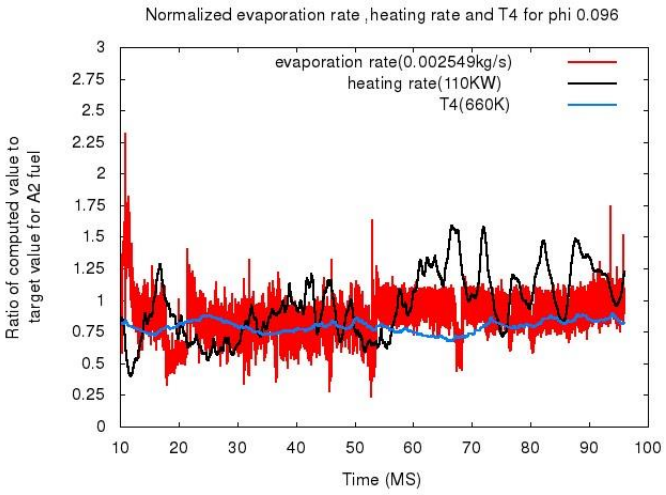


**FIGURE 19** Temporal efficiency of Cat-A2 fuel evaporations, heating rate and $T_4$ at $\phi$=0.096.

The flow split between the three swirlers and the two rows of the dilution holes is computed and is shown with heating rate in the (a) and (b) panels of Figure 20.

The total mass flow of all three swirlers that enters the forward combustor is about 17.82% (69.69 G/S) of the inlet mass which is larger than that of 15.9% (62.2 G/s) of the inlet mass for the non-reacting case. The effective equivalence ratio from all the swirler flowrate is about 0.51. The primary equivalence ratio from the swirler flowrate, a quarter of the first dilution jet flowrate and the dome effusive cooling flowrate is around 0.37. The total mass flowrate of all two dilution rows that enter the combustor, forward and aft, is 23.93% (93.57 G/S) of the inlet mass which is larger than that of the non-reacting mass flow, 22.4% (87.6 G/S) of the inlet mass.

It is very clear that the unsteady heating rate and the unsteady flow split for the three swirlers and two rows of the dilution holes have the near 180° out-of-phase relationship. The phase difference is the same as that between acceleration and displacement in a simple harmonic vibration.

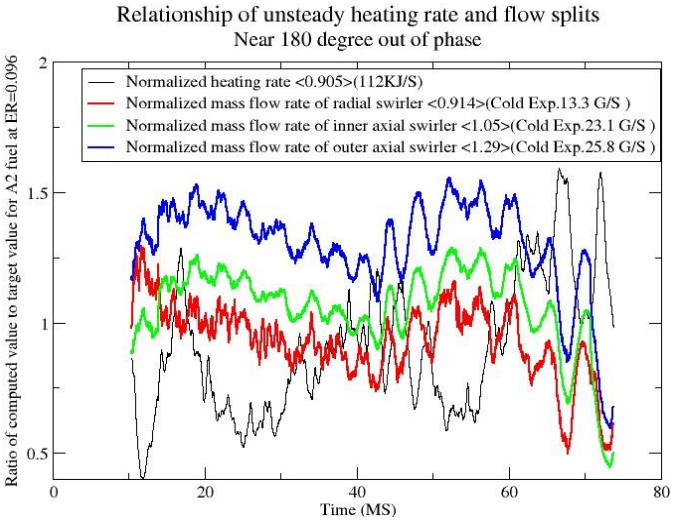


**(a)**

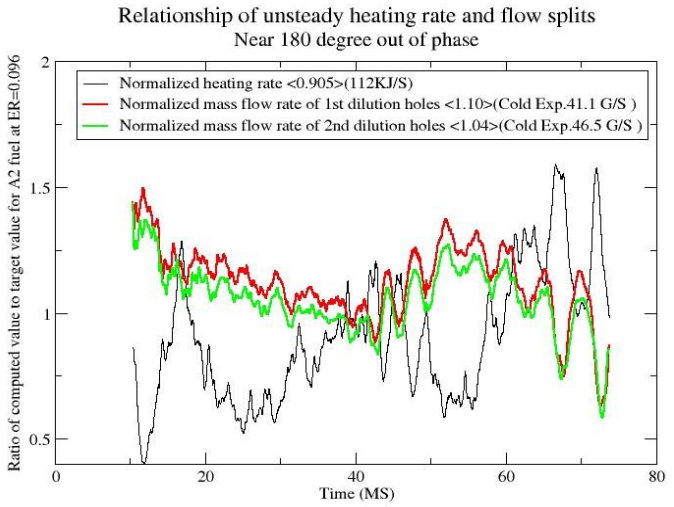


**(b)**

**FIGURE 20** 180° out-of-phase relationship between temporal efficiency of heating rate and flow splits for ϕ=0.096 Cat-A2 fuel (a) three swirlers (b) two dilution rows.

Simulations with reduced equivalence ratio, ϕ=0.088 starts around 37 MS from the results of ϕ=0.096. Then the equivalence ratio steps down to 0.085 after 10 MS stable simulations of ϕ=0.088. After another 10 MS stable simulations, the equivalence ratio steps down to 0.085. After another 8.8 MS stable simulations of ϕ=0.085, the equivalence ratio steps down to 0.082. After 7 MS with ϕ=0.082 the unsteady heating rate reduces to around 0.7 KW which is about 99.3% lost compared to the targeted value, 95 KW. The approach to LBO is achieved when the equivalence ratio is 0.082 for Cat-A2 fuel.

The LBO equivalence ratio from the experimental data is between 0.080 and 0.079. In Figure 21, the normalized unsteady heat release rates at different step-wise equivalence ratio are shown. The instantaneous temperature contours with different ϕ from 0.096 to 0.082 are shown in Figure 22.

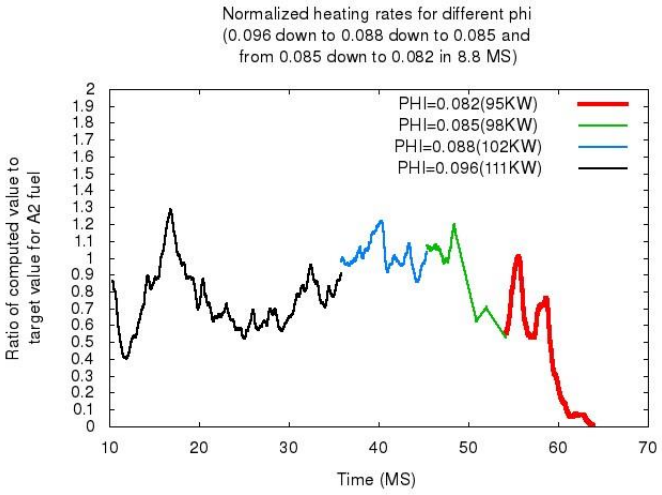


**FIGURE 21** Normalized temporal heating rates of Cat-A2 fuel with step-down $\phi$. (Step down from 0.085 to 0.082 in 8.8MS.)

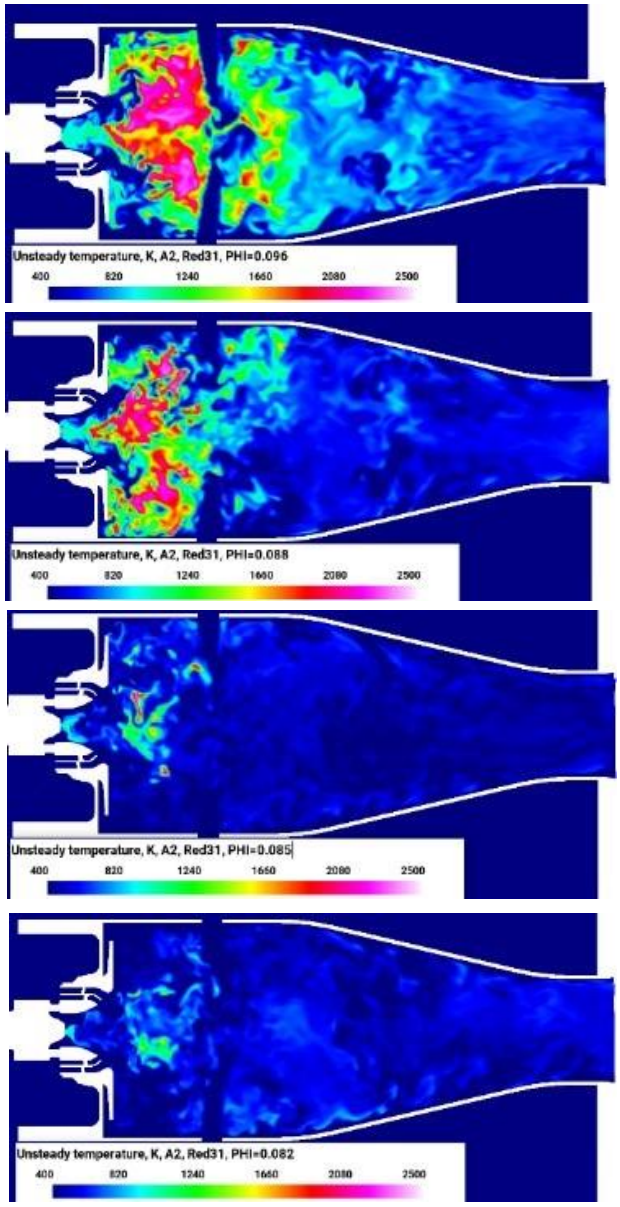


**(a)**

**(b)**

**(c)**

(d)

**FIGURE 22** Instantaneous center-plane temperature contours at (a) $\phi$=0.096 (b) $\phi$=0.088 (c) $\phi$=0.085 (d) $\phi$=0.082

In Figure 23, the normalized unsteady evaporation rates at different step-wise equivalence ratio are shown. (Note: the targeted evaporation rate is different from each other.)

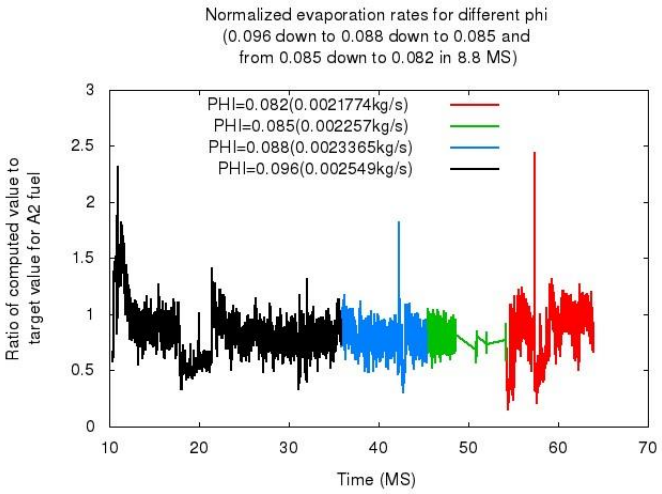


**FIGURE 23** Normalized temporal fuel evaporation rates of CatA2 fuel with step-down ϕ. (Step down from 0.085 to 0.082 in 8.8MS.)

Since LES predicted LBO equivalence ratio, 0.082, is higher than that of the experimental equivalence ratio, 0.079705 ~ 0.081495, it is speculated that stepping down from ϕ=0.085 to ϕ =0.082 in 8.8 MS could be the reason.
To understand proper step-down process, i.e. to assess the impact of the time span of each equivalence ratio, LES simulation with equivalence ratio 0.085 was restarted and sustained for another 21 MS, total is 30 MS, then to step down to ϕ=0.082. The stepdown process continues to ϕ = 0.081 and to ϕ = 0.078. In Figure 24, the normalized unsteady heat release rates at different step-wise equivalence ratio with longer span for ϕ=0.085 are shown. It indicates that with longer span for ϕ=0.085the approach to LBO occurs at the equivalence ratio of 0.078.

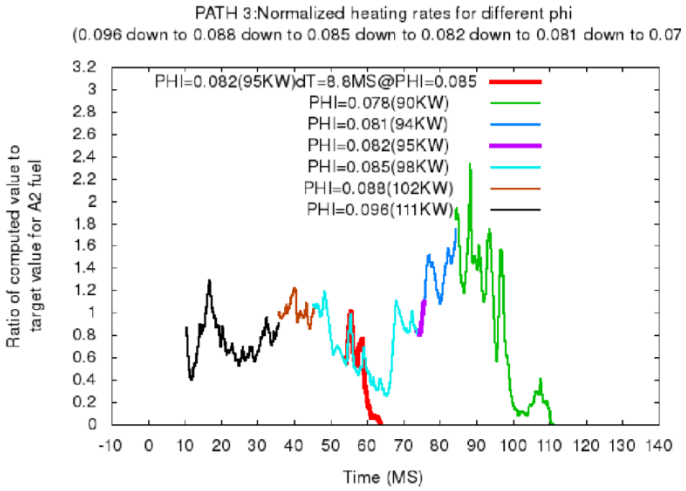


**FIGURE 24** Normalized temporal heating rates of Cat-A2 fuel with step-down ϕ. (Step down from 0.085 to 0.082 in 30 MS versus step down from 0.085 to 0.082 in 8.8 MS.)

In Figure 25, the normalized unsteady evaporation rates at different step-wise equivalence ratio are shown.

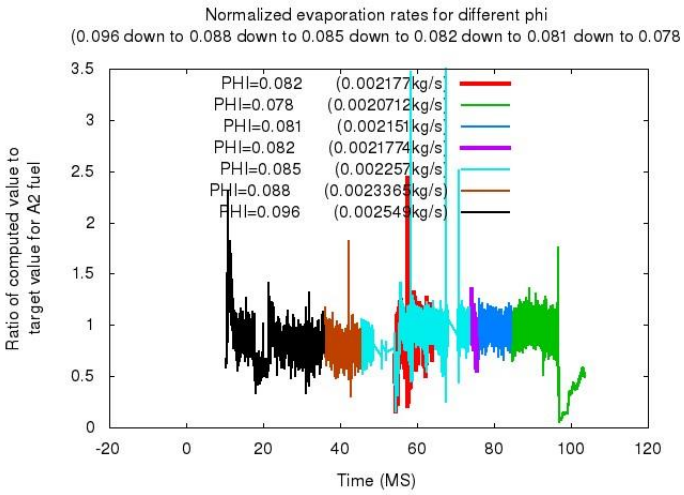


**FIGURE 25** Normalized temporal fuel evaporation rates of CatA2 fuel with step-down ϕ. (Step down from 0.085 to 0.082 in 30 MS.)

## 3. CONCLUSION

In this paper, the strategy of using K-LES in analyzing the sensibility of two aviation fuels in a referee combustor rig that is a single-cup, swirl-stabilized RQL (rich-burn, quick-mix, lean-burn) combustor was developed. An average jet fuel (denoted as "Cat-A2" in the NJFCP) and a test fuel (Cat-C1) were selected for the sensitivity study.

LES simulations with consecutive decreased equivalence ratios were performed to examine the combustion characteristics starting at stable conditions near lean blow-out to lean blow-out in order to understand the trend of the stabilization mechanisms.

It was observed that at ϕ=0.096 the unsteady heating rate and the unsteady flow split for the three swirlers and two rows of the dilution holes have the 180° out-of-phase relationship like acceleration and displacement in a simple harmonic vibration.

For Cat-C1 fuel, LES simulations predict LBO occurring at 0.087 <= < 0.090. For Cat-A2 fuel, the LBO from LES occurs at 0.082 <= ϕ < 0.085 only if the simulation is stepped down from an 8.8MS simulation at ϕ=0.085. The predicted difference in LBO for Cat-C1 relative to Cat-A2 was |0.087-0.082|/0.082 = 0.061, compared to the experimental value of |0.08690.0806|/0.0806 = 0.078, where 0.0869 was the mean value between 0.08614 and 0.087660 for Cat-C1 fuel, while 0.0806 is the mean value between 0.079205 and 0.081455 for Cat-A2 fuel. However if the approach to LBO simulation for A2 was stepped down from a 30MS run at ϕ =0.085, the prediction of LBO for A2 was 0.082. The predicted difference in LBO for Cat-C1 relative to Cat-A2 is |0.087-0.078|/0.078 = 0.115. Summary of OpenNCC LBO predictions vs experiments is shown in Table 3.

| | **A2 LBO** | **C1 LBO** | **Fuel relative diff in LBO : $(\phi_{C1} - \phi_{A2})/\phi_{A2}$** | **Comment** |
|---|---|---|---|---|
| **OpenNCC** | **0.078 (0.082)** | **0.087 0.087** | **11.54% (6.10%)** | **30MS for ϕ=0.085 (9 MS for ϕ=0.085)** |
| **Experiment** | **0.0806**<br><br>**0.0788 to 0.0824 (40 runs)** | **0.0869**<br><br>**0.08535 to 0.0884 ( 20 runs)** | **3.58% 7.77% 12.51%**<br><br>**MIN. AVG. MAX** | **MIN = (0.08532-0.0824)/0.0824=3.58%**<br><br>**MAX= (0.0884-0.0788)/0.0788=12.15/%** |

Table 3 Summary of OpenNCC LBO predictions vs experiments.

To further assess the impact of the span of the equivalence ratio in the step-down process, LES simulations not using source/sink model of the effusion flux are needed and are the ongoing efforts.

## ACKNOWLEDGEMENTS

This work was supported by the NASA Transformational Tools and Technologies (TTT) project under the Transformative Aeronautics Concepts (TACP) program.

## REFERENCES

[1] Stouffer, Scott, et. al, "Lean Blowout and Ignition Characteristics of Conventional and Surrogate Fuels Measured in a Swirl Stabilized Combustor", *55th AIAA Aerospace Sciences Meeting*. AIAA-2017-1954.

[2] Colket, M., "An overview of the National Jet Fuels Combustion Program", *54th AIAA Aerospace Sciences Meeting*. AIAA-2016-0177.

[3] Edwards, T., "Reference Jet Fuels for Combustion Testing", *55th AIAA Aerospace Sciences Meeting*. AIAA-20170146.

[4]Kitamura, K, et. al, "A New Pressure Flux for AUSMFamily Scheme for Hypersonic Heating Computations," 2010 AIAA Computation Fluid Dynamics Conference. AIAA 20113030.

[5] Frossling, N., "ber die Verdunstung Fallender Tropfen," Gerlands Beitrge zur Geophysik, Vol. 52, 1938, pp.170-215.

[6] Faeth, G. M. "Evaporation and Combustion of Sprays," Prog. in Energy and Comb. Sci., 9,1 (1983)

[7] Wey, C. T., " Fuel Sensitivity of Lean Blowout in a RQL Gas Turbine Combustor," AIAA 2019 Propulsion and Energy Forum. AIAA 2019-4035.

[8] Wang, H., Xu, R., Wang, K., Bowman, C. T., Davidson, D.F., Hanson, R. K., Brezinsky, K., Egolfopoulos, F. N., "A physics-based approach to modeling real-fuel combustion chemistry - I. Evidence from experiments, and thermodynamic, chemical kinetic and statistical considerations," Combustion and Flame 193 (2018) 502-519.

[9] Esclapez, L., Ma, P. C., Mayhew, E., Xu, R., Stouffer,
S., Lee, T., Wang, H., Ihme, M., "Fuel Effects on Lean BlowOut in a Realistic Gas Turbine Combustor," Combustion and Flame 181 (2017) 82-99.